



# Uncertainties in aerosol direct and indirect effects attributed to uncertainties in convective transport parameterizations

T. Storelvmo

Yale University, Department of Geology and Geophysics, New Haven, CT, USA

## ARTICLE INFO

### Article history:

Received 7 January 2011

Accepted 29 September 2012

### Keywords:

Aerosols

Black carbon

Clouds

Entrainment

Regional climate

## ABSTRACT

Deep convection is an important transport mechanism for aerosol particles, allowing them to be lifted to levels where they are subject to long-range transport from source regions to remote regions. The sensitivity of regional aerosol effects to the rate of entrainment in deep moist convection has been explored in a global modeling framework, and found to be crucial for the radiative balance both at the surface and at the top of the atmosphere. The fact that regions where deep convection is frequent often coincide with regions of particularly high black carbon emissions is found to be an important factor in understanding this sensitivity to entrainment. More entrainment leads to shallower convective plumes and less aerosol transport from the boundary layer to the upper troposphere in source regions. As a result, boundary layer aerosol concentrations are increased in source regions, while upper tropospheric aerosol concentrations are reduced globally. This generally leads to stronger aerosol effects in polluted regions and weaker aerosol effects in remote regions. Because black carbon particles have the ability to absorb solar radiation, reducing their concentration leads to more solar radiation reflected back to space, especially over bright surfaces. Conversely, at the surface more entrainment means more downwelling shortwave radiation everywhere but in source regions. Regions that experience increased aerosol concentrations in the boundary layer in response to increased entrainment observed a stronger aerosol indirect effect, while the opposite was true everywhere else. This study highlights that the relative strengths of the aerosol direct and indirect effects in clean versus polluted regions depend crucially on the rate of entrainment in deep convective clouds, a process that is presently not well understood and quantified.

© 2012 Elsevier B.V. All rights reserved.

## 1. Introduction

Despite intense research in recent decades, the uncertainties associated with aerosol effects on Earth's climate variability are larger than ever. Human activity has substantially perturbed the atmospheric loading of aerosol particles since preindustrial times, and climate models currently predict the global mean anthropogenic aerosol influence on climate to cause everything from a negligible cooling to one comparable in magnitude to the warming from increasing greenhouse gas (GHG) concentrations (Forster et al., 2007). Climate change can not be predicted with confidence until this uncertainty range has been narrowed.

Aerosols affect climate *directly* by scattering and absorbing solar radiation, and *indirectly*, by acting as nuclei for cloud droplet or ice crystal formation, thereby perturbing cloud albedo and lifetime. In contrast to the globally uniform increase in GHG concentrations, the concentration of aerosol particles is highly variable in space and time, because the atmospheric lifetimes of aerosols and GHGs differ by orders of magnitude. The sum of the two major drivers of anthropogenic climate change will thus be dramatically different from one region to another, and largely determined by the spatial and temporal variations in aerosols. Hence, in order to predict regional climate change, an accurate treatment of aerosol transport mechanisms and lifetimes in global climate models is essential.

Deep convection is crucial as a vertical transport mechanism of aerosol from the surface, where they are emitted, to the upper

E-mail address: [trude.storelvmo@yale.edu](mailto:trude.storelvmo@yale.edu).

troposphere where longer atmospheric lifetimes and long-range transport are possible. The amount of entrainment is one of the key factors determining to which level in the troposphere a convective plume penetrates and detains water and pollutants. Hence, it is alarming that global climate models have repeatedly been reported to poorly represent convective entrainment and detrainment (Grabowski and Moncrieff, 2004; Maloney et al., 2010). For example Grabowski et al. (2006) compared single-column model (SCM) versions of two GCMs and several cloud-resolving models (CRMs) to observations of a developing convective cloud in Amazonia. Compared to the observations and the 3D CRMs, the SCMs developed deep convection too early, likely due to too weak entrainment (e.g. Del Genio and Wu, 2010).

Another highly uncertain aspect of moist convection in global models is the convective precipitation release. Wet removal is the main removal process for atmospheric aerosol, and controls the fraction of aerosols in a convective plume reaching the upper troposphere. A study by Textor et al. (2006) found strong disagreement among GCMs in the fraction of aerosol wet removal caused by convective precipitation (ranging from 10% to 90%). Convective precipitation is partly controlled by the entrainment of dry environmental air into the moist convective plume, a process which tends to reduce rainfall.

A novel approach in climate modeling is so called “super-parameterization”, in which GCMs are coupled to cloud-resolving models, thereby avoiding the use of parameterization schemes for deep convection entirely (Grabowski, 2001; Gustafson et al., 2008). While showing great promise, such multi-scale modeling frameworks are computationally very expensive, and therefore presently not suitable for the long model integrations required for projections of future climate.

This study seeks to demonstrate how sensitive regional aerosol effects are to the entrainment in deep convective clouds. GCM studies of aerosol direct and indirect effects have to date often focused on aerosol perturbations to the global mean climate, disregarding the strong regional contrasts. As will be demonstrated in this study, changes in deep convective entrainment yield opposing effects in source regions and remote regions. This is of relevance for prediction of regional climate change, and in particular the contrast in warming between low and high latitudes.

The remainder of this paper is structured as follows: Section 2 describes the modeling tool used in this study, focusing particularly on the parameterization scheme for deep convection and the treatment of aerosols in the model. Section 3 presents and discusses the simulated aerosol concentrations and related effects on radiation, and finally Section 4 presents some further discussion and conclusions.

## 2. The modeling tool and approach

### 2.1. NCAR CAM and its convection scheme

The modeling tool in this study is a modified version of the National Center for Atmospheric Research (NCAR) Community Atmosphere Model (CAM), Version 3 (Collins et al., 2006). A more recent version of NCAR CAM is now available, but there are few changes in the treatment of deep convection between the two model versions. However, Convective Available

Convective Energy (CAPE) is calculated differently in the most recent version, as will be discussed in more detail below. Furthermore, for the purpose of studying aerosol-climate interactions, NCAR CAM3 has been modified with i) a sophisticated aerosol life cycle scheme with a hybrid modal/bin aerosol microphysics (Seland et al., 2008), and ii) a two-moment cloud microphysics scheme of complexity comparable to the cloud microphysics in NCAR CAM5 (Storelvmo et al., 2006). Hence, the modeling tool is suitable for the present study. Description of the convection scheme and the modified treatment of aerosols and their interaction with clouds and radiation follow below.

For the present study, the modified NCAR CAM3 was integrated on a T42 spectral truncation, with a physical timestep of 30 min and 26 vertical layers. Each of the simulations was integrated for one year, after four months of initial model spin-up. Of particular relevance for this study is the treatment of deep moist convection, which follows the parameterization of Zhang and McFarlane (1995). The scheme is based on a plume ensemble approach, where it is assumed that an ensemble of convective updrafts may exist whenever the atmosphere is conditionally unstable in the lower troposphere. The updraft ensemble is represented by a collection of entraining plumes, each with a characteristic and constant fractional entrainment rate  $\lambda$ . It is further assumed that all updrafts start at the same base level and that the updraft base mass flux is evenly distributed. These assumptions allow for a simplified, bulk formulation (BF) type calculation of convective mass fluxes, summing the contributions from each individual plume. Aerosols and aerosol precursors transported upward by the convective plumes are detrained into the environment in a thin layer at the top of the plume,  $Z_d$ . The smaller  $bda$ , the larger  $Z_d$ . The ensemble cloud updraft mass flux is given by

$$M_u = \left( \frac{M_b}{\lambda_0(Z_d - Z_b)} \right) \left( \exp(\lambda(Z_d)(Z_d - Z_b)) - 1 \right) \quad (1)$$

where  $\lambda_0$  is the entrainment rate of the shallowest plume in the ensemble (and hence the plume with the highest entrainment rate),  $Z_b$  is the height of the cloud base, and  $M_b$  is the updraft mass flux at cloud base. The closure assumption for this convection scheme is that CAPE is consumed at an exponential rate by cumulus convection. This assumption implies that

$$M_b = \frac{\text{CAPE}}{\tau F} \quad (2)$$

where  $F$  is the CAPE consumption rate per unit cloud base mass flux and  $\tau$  is the characteristic time scale of convection, in this model set to 7200 s. In the original scheme, CAPE was calculated for undiluted air parcels, while in CAM5 parcel dilution is accounted for in the CAPE calculations, following the approach of Raymond and Blyth (1986) and Raymond and Blyth (1992). Allowing for plume dilution will act to decrease CAPE, and hence the mass flux at cloud base, according to Eq. (2). Hence, one would expect slightly weaker convective updrafts with the modified scheme, and therefore possibly a weaker effect of modified entrainment than what is found in the present study. Convective precipitation release is controlled by the following equation

$$R_r = C_0 M_u l \quad (3)$$

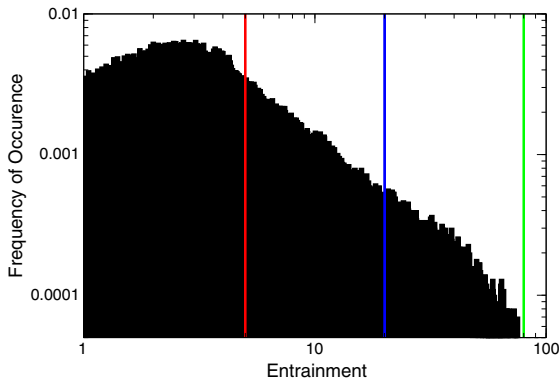


**Fig. 1.** Probability density function for fractional entrainment rate ( $10^{-5} \text{ m}^{-1}$ ) for the shallowest moist convective plumes over a randomly chosen 24-hour simulation period. Vertical lines represent the default maximum entrainment rate in NCAR CAM (blue), and the corresponding quantity chosen for sensitivity simulations  $ENT_{HIGH}$  (green) and  $ENT_{LOW}$  (red), respectively.

where  $l$  is the ensemble mean in-cloud convective cloud water and  $C_0$  is a constant equal to  $3 \cdot 10^{-3} \text{ m}^{-1}$ . Evident from Eqs. (1) and (2) is that when  $\lambda_0$  is increased (decreased), the mass flux is decreased (increased) and the convective precipitation is decreased (increased). The maximum fractional entrainment rate,  $\lambda_0$ , is set by identifying the level of minimum moist static energy for a saturated state, typically in the middle troposphere. The shallowest convective plume is required; to detrain above this level, which in turn constrains the entrainment of this plume. Fig. 1 shows  $\lambda_0$  as predicted by the convection scheme, sampled from all convective ensembles present globally within a randomly sampled 24-hour period of model simulation. In the standard CAM3 (and also the more recent CAM5), the maximum allowed fractional entrainment rate for any plume is set to  $0.0002 \text{ m}^{-1}$ , indicated by the blue vertical line in Fig. 1. As evident in Fig. 1, the convection scheme frequently predicts

fractional entrainment rates higher than this maximum value. This is confirmed by Fig. 2, showing annual mean  $\lambda_0$  values from a simulation with no upper bound on this parameter. Evident are several regions where even the annual mean  $\lambda_0$  is above  $0.0002 \text{ m}^{-1}$ . As discussed in Section 1, there are very few observational constraints available for entrainment in deep moist convection. Laboratory and cloud modeling studies seem to agree that an entrainment rate of  $\lambda = \frac{0.2}{R}$ , where  $R$  is the radius of the convective plume, is a good approximation (Pruppacher and Klett, 1997). With this approximation, a plume with a radius of 100 m would yield an entrainment rate of  $2 \cdot 10^{-3} \text{ m}^{-1}$  and a radius of 10 km would yield an entrainment rate of  $2 \cdot 10^{-5} \text{ m}^{-1}$ . Combining this with cloud geometries from satellite data (e.g. Benner and Curry, 1998) or from Large Eddy Simulations (LES) (e.g. Siebesma and Jonker, 2000) could provide empirical guidance for entrainment rates, given a convective plume height. Presumably, an ensemble of convective plumes of different heights would also represent a range of convective plume radii, and there seems to be no justification in the literature for the choice of one *maximum* entrainment rate (currently  $2 \cdot 10^{-4} \text{ m}^{-1}$ ) valid for all plumes.

Convective transport is of importance for a range of processes in the atmosphere, examples being atmospheric chemistry (Mahowald et al., 1997) and the transport of water vapor to the upper troposphere and lower stratosphere. Lawrence and Rasch (2005) compared the convective transport of short-lived chemical tracers using two different approaches for the calculation of convective mass fluxes: the BF approach described above and a true Plume Ensemble Formulation (PEF) where fluxes are calculated for each individual plume. They found that for short-lived tracers (lifetime <5 days), the BF significantly underestimates the transport to the upper troposphere compared to the PEF, mainly because the existence of undiluted plumes cannot be properly accounted for with the BF approach. Recently, it has been demonstrated that aerosols may in fact influence the entrainment rate in shallow cumulus

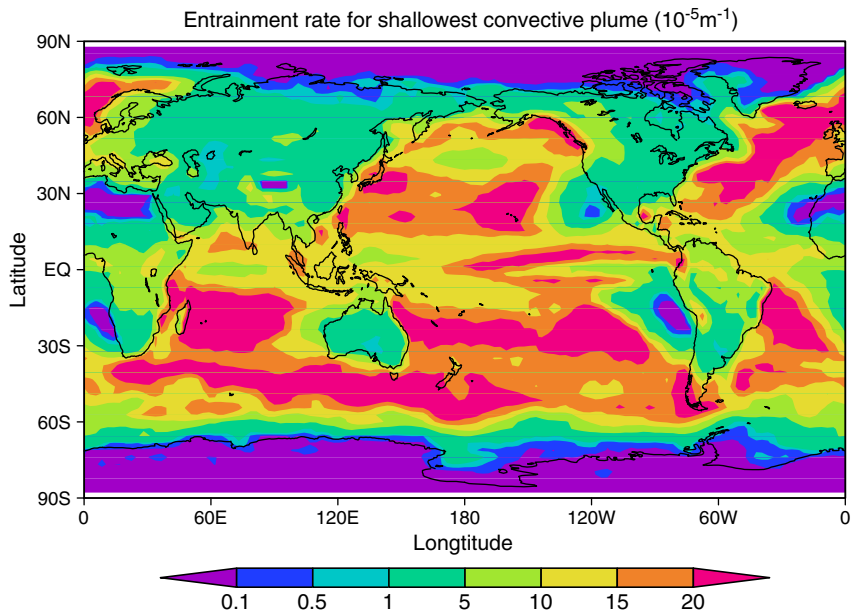


**Fig. 2.** Annual mean fractional entrainment rate ( $10^{-5} \text{ m}^{-1}$ ) for the shallowest moist convective plume in the grid box ensemble.

clouds, and thereby modify their lifetime (Small et al., 2009). Here we focus on the entrainment in deep moist convection as a controlling factor for aerosol transport and lifetime, and seek to demonstrate that uncertainties in convective entrainment rates ultimately translate into uncertainties in aerosol effects on climate.

## 2.2. Treatment of aerosols and their interaction with clouds and radiation

The aerosol treatment in this study follows Seland et al. (2008), and treats the following aerosols and aerosol precursors as prognostic variables: sulfate, sea salt, mineral soil dust, particulate organic matter (POM), black carbon (BC) and the gaseous precursors di-methyl-sulphide (DMS) and sulphur dioxide (SO<sub>2</sub>). Aerosol emissions are taken from Dentener et al. (2006), and all aerosol components are emitted from ground-based sources, but are distributed vertically at the time of emission following the recommendations by Dentener et al. (2006). Primary particles are emitted in an initial size distribution described by a superposition of 11 lognormal modes (3 sea salt, 2 mineral dust, 2 SO<sub>4</sub>, 2 BC, 1 OM and 1 OM/BC). The size distribution is subsequently modified by condensation and coagulation processes using 44 size bins in the radius range 0.001–20 μm, allowing for both external and internal mixing, and deviations from the lognormal form.

Aerosol optical properties are calculated based on the modified size distribution with the use of look-up-tables, to save computing time (Kirkevåg and Iversen, 2002). The cloud droplet number concentration is predicted based on the modified aerosol size distribution following Storelvmo et al. (2006). Cloud droplet activation follows Abdul-Razzak and Ghan (2000) and is based on a sub-grid distribution of vertical velocity and hence supersaturation.

## 2.3. Experimental approach

To explore the sensitivity to entrainment in deep convection, the following simulations have been carried out: (i) Simulation *CTL*: A control simulation without modifications to the convection, (ii) Simulation *ENT<sub>LOW</sub>*, which has a stronger constraint on the maximum entrainment allowed for each individual convective plume, and iii) Simulation *ENT<sub>HGH</sub>* which has a weaker constraint on the maximum entrainment for each convective plume. The red and green vertical lines in Fig. 1 represent the maximum values that were chosen for the

sensitivity simulations *ENT<sub>HGH</sub>* and *ENT<sub>LOW</sub>*. The values are arbitrary, but certainly within the range of uncertainty associated with entrainment in deep convective clouds. Each simulation is carried out twice; once with emissions of aerosols and aerosol precursors corresponding to present day (PD), and once with preindustrial (PI) emissions. In each simulation, offline calculations of the direct and indirect aerosol effects are calculated by calling the radiation routine three times: One call for calculations of the direct aerosol effect, another call for calculations of the indirect aerosol effect and a final call with prescribed default NCAR CAM3 aerosol and cloud droplet concentrations, used for model integration, ensuring identical meteorologies in the PD and PI simulations. The offline calculations are advantageous because the observed changes in the radiative balance can be directly attributed to the changes in aerosols, without the various complex feedbacks on atmospheric circulation that often make GCM results difficult to interpret. The disadvantage is that the above mentioned feedbacks in response to aerosol radiative forcings take place in nature as well, so by disregarding them we do not allow for the full atmospheric response to aerosol perturbations but rather their pure radiative forcings. For a more thorough discussion on this topic, see for example (Lohmann et al., 2010) and (Stevens and Feingold, 2009).

## 3. Results

### 3.1. Changes in aerosol loadings and distributions in response to modified entrainment

Table 1 summarizes the vertically integrated atmospheric loadings for BC, POM, sulfate, sea salt and mineral dust in simulation *CTL*, as well as the difference in aerosol loadings between simulations *ENT<sub>HGH</sub>* and *ENT<sub>LOW</sub>*. In addition to global mean aerosol loadings, values averaged over the Tropics (30°N–30°S), the Northern Hemisphere (NH, 30°N–90°N) and Southern Hemisphere (SH, 90°S–30°S) are also given in Table 1. Evident is the relatively large reductions in BC and POM loadings, particularly in the Tropics and NH, when entrainment is increased. BC and POM lifetimes in *ENT<sub>LOW</sub>* are 5.9 and 6.3 days, respectively, while in *ENT<sub>HGH</sub>* they are significantly increased, to 7.1 and 7.9. Similar changes in BC lifetime have previously been reported in Barth and Church (1999) in response to different transfer rates from hydrophobic to hydrophilic BC. For the aerosol module applied in this study, an e-folding time of 1 day for the conversion from hydrophobic to

**Table 1**

Global and annual average column burden (CB) from control simulation for black carbon (BC), particulate organic matter (POM), sulfate (SO<sub>4</sub>), sea salt (SS) and mineral soil dust (DU), and changes in CBs between simulation *ENT<sub>HGH</sub>* and *ENT<sub>LOW</sub>*. Tropics refers to the 30°N–30°S mean, NH refers to the 30°N–90°N mean and SH to the 90°S–30°S mean.

Aerosol column burden					
Aerosol type	BC (mg/m <sup>2</sup> )	POM (mg/m <sup>2</sup> )	SO <sub>4</sub> (mg S/m <sup>2</sup> )	SS (mg/m <sup>2</sup> )	DU (mg/m <sup>2</sup> )
CB, Global	0.246	2.24	1.11	9.76	35.7
CB, Tropics	0.297	3.0	1.06	6.30	45.4
CB, NH	0.292	1.90	1.85	8.42	45.7
CB, SH	0.097	1.07	0.495	18.0	6.09
ΔCB, Global	0.049 (20%)	0.546 (24%)	0.151 (14%)	0.676 (6.9%)	2.66 (7.4%)
ΔCB, Tropics	0.060 (20%)	0.687 (23%)	0.158 (15%)	0.331 (5.3%)	2.22 (4.9%)
ΔCB, NH	0.056 (19%)	0.511(27%)	0.233 (13%)	0.336 (4.0%)	5.39 (11.8%)
ΔCB, SH	0.020 (20%)	0.301(28%)	0.054 (11%)	1.71 (9.5%)	0.783 (12.9%)

hydrophilic BC has been calculated, and the conversion was found to be dominated by coagulation (Seland et al., 2008). This is similar to values calculated for an urban plume during night time reported in a recent study with a particle-resolving aerosol model (Riemer et al., 2010). The same study reported much higher and condensation-dominated aging rates during daytime, but these were calculated for very polluted conditions.

A more moderate relative reduction in sulfate loading, and even smaller relative reductions in sea salt and dust loadings are also found in response to increased entrainment. Sea salt and dust particles are largely coarse mode particles which are efficiently scavenged, and their loadings are therefore less sensitive to convective transport. Increased entrainment of dry environmental air in moist convective plumes reduces the plume height and the level of detrainment, as well as the upward mass flux. Consequently, aerosol concentrations in the planetary boundary layer and the lower free troposphere will be increased close to sources, while the upper troposphere globally and the lower troposphere in remote regions experience reduced aerosol concentrations in response to the increased entrainment.

Fig. 3a–c shows the annual and zonal mean changes in anthropogenic BC, POM and sulfate between simulations  $ENT_{HGH}$  and  $ENT_{LOW}$ . While changes in POM and BC occur in both hemispheres, the changes in sulfate mass mixing ratio are largely confined to the NH, where anthropogenic sulfur emissions are larger. High emissions of BC and POM from biomass and fossil fuel burning often correspond with regions of high moist convective activity in both hemispheres, hence their relatively large sensitivity to moist convective transport.

From Eqs. (1) and (2), one would expect less convective precipitation in simulation  $ENT_{HGH}$  than in simulation  $ENT_{LOW}$ . Reduced convective precipitation would lead to less wet scavenging of aerosols, and thus increased aerosol concentrations, opposing the effect of the reduced mass flux. Convective rainfall is indeed reduced in simulation  $ENT_{HGH}$  versus  $ENT_{LOW}$ , but the reduction only amounts to a relatively modest 2% globally averaged, and the convective transport mechanism seems to be the dominant one in this study.

### 3.2. Aerosol direct and indirect effects in the control simulation

Fig. 4a shows the aerosol direct effect at the top of the atmosphere (TOA) from simulation  $CTL$ . Over regions with bright surfaces and high cloudiness, anthropogenic aerosols cause a perturbation to the radiation budget at the TOA. This is particularly true in regions where the ratio of absorbing to scattering aerosols is large. In contrast, over darker surfaces anthropogenic aerosols increase solar radiation scattered back to space, and hence cool the Earth–atmosphere system. As evident from Table 2, the global and annual average is negligible, while regional effects, somewhat represented by the values for the Tropics, the NH and SH, show significant radiative forcings of both signs. The slightly positive global mean aerosol direct effect at the TOA of  $0.01 \text{ W m}^{-2}$  found here is in the upper part of the range reported for multiple global aerosol models using the same set of emissions ( $-0.41$ – $0.04 \text{ W m}^{-2}$  (Schulz et al., 2006)). As discussed in (Seland et al., 2008), this is intimately connected to the simulated aerosol size distribution and degree of external versus internal aerosol mixing.

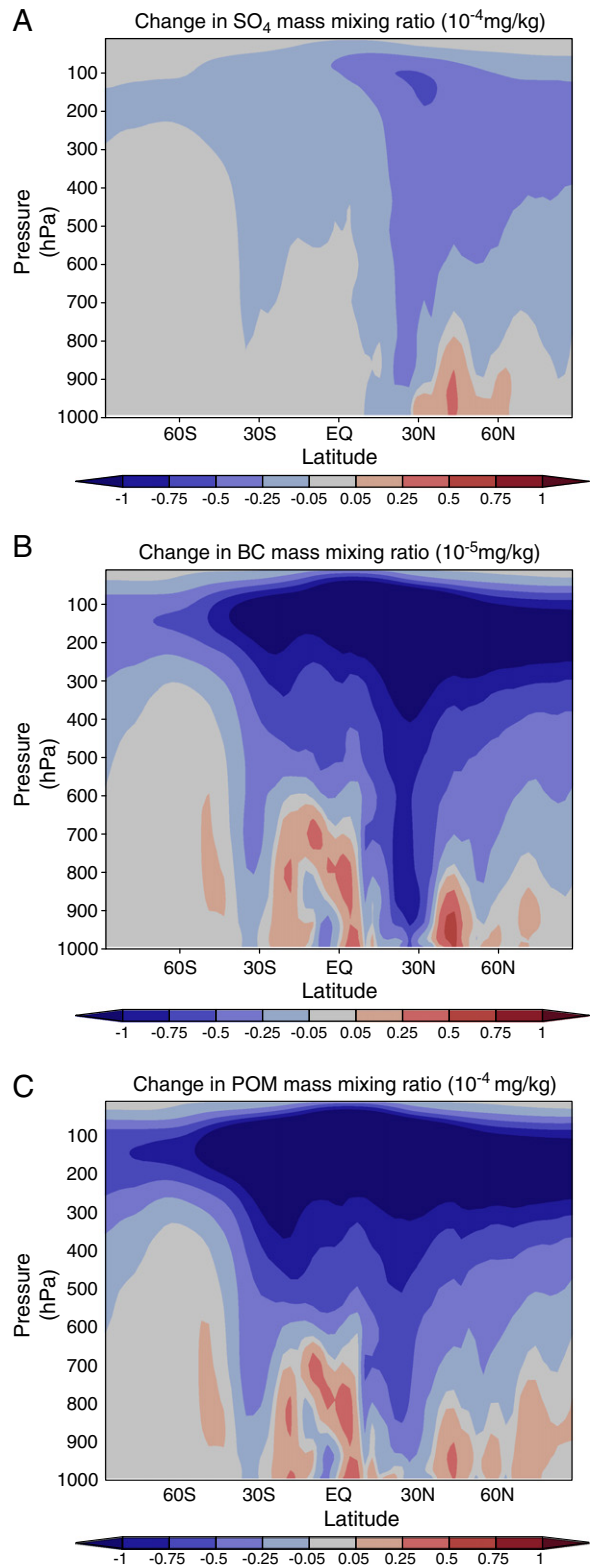
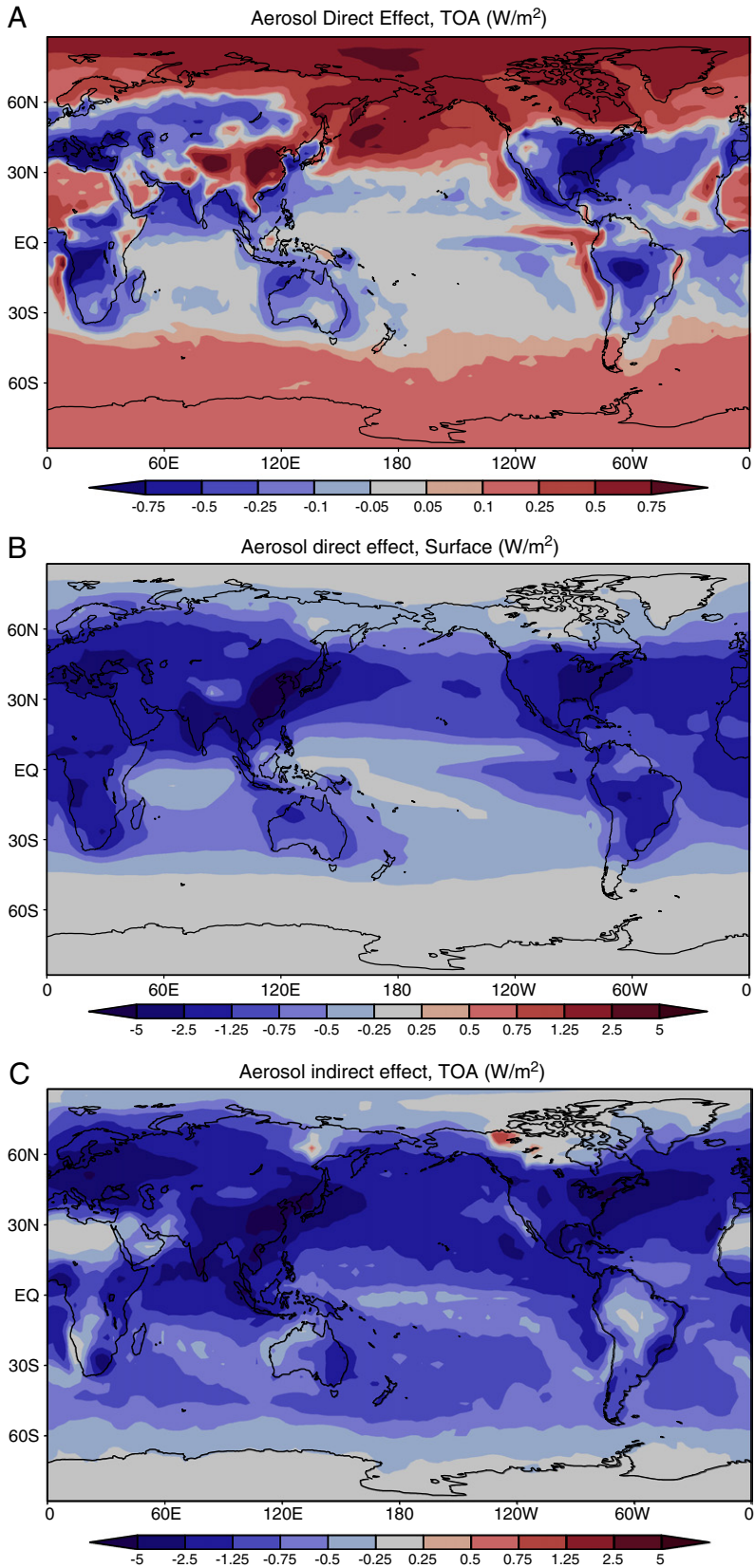


Fig. 3. Zonal and annual averages of changes in aerosol mass mixing ratio in response to increased entrainment in deep convective clouds ( $ENT_{HGH} - ENT_{LOW}$ ): a) SO<sub>4</sub>, b) BC and c) POM.



**Table 2**

Global and annual mean aerosol direct and indirect effects (ADE and AIE, respectively) in the control simulation, and changes in ADE and AIE between simulation  $ENT_{HGH}$  and simulation  $ENT_{LOW}$ .

Aerosol direct and indirect effects				
Forcing	Global	Tropics	NH	SH
ADE, TOA ( $W m^{-2}$ )	0.01	−0.10	0.15	0.08
ADE, Surface ( $W m^{-2}$ )	−0.98	−1.11	−1.42	−0.17
AIE ( $W m^{-2}$ )	−1.27	−1.24	−1.97	−0.61
$\Delta$ ADE, TOA ( $W m^{-2}$ )	0.03	0.02	0.09	0.01
$\Delta$ ADE, Surface ( $W m^{-2}$ )	0.15	0.27	0.16	0.07
$\Delta$ AIE ( $W m^{-2}$ )	0.11	0.22	0.04	0.02

Because the aerosol direct effect can be vastly different at the TOA and at the surface, the aerosol direct effect at the surface is shown in Fig. 4b. It is, as expected, negative everywhere, strongest over source regions and weakest at high latitudes, particularly in the SH. Maxima are located over source regions, most notably North-East Asia, Eastern USA and Europe. On a global and annual average, anthropogenic aerosols reduce the net downward radiation at the surface by  $\sim 1 W m^{-2}$  (Table 2). This estimate is very similar to the mean surface forcing of all models reported in (Schulz et al., 2006).

A similar geographic forcing distribution is evident from Fig. 4c, showing the aerosol indirect effect, accounting for changes in cloud albedo only. However, controlling factors for the aerosol indirect effect are: i) the collocation of anthropogenic aerosols and clouds, hence the low forcing values over Sahara. ii) Pristine environments with low cloud condensation nuclei (CCN) concentrations are more susceptible to anthropogenic CCN perturbations than are polluted environments, hence the relatively strong aerosol indirect forcings over oceans, particularly over the North Pacific. On a global and annual average, the cloud albedo effect amounts to  $-1.27 W m^{-2}$  in the CTL simulation (Table 2). This is well within the range of values obtained from a survey of published global estimates of the cloud albedo effect, yielding a mean of  $-0.94 W m^{-2}$  and a standard deviation of  $0.43 W m^{-2}$  (updated estimate from (Lohmann et al., 2010)).

### 3.3. Relative contributions from BC, POM and $SO_4$ to the direct and indirect aerosol effects

Fig. 5 displays the relative contributions to the total aerosol direct and indirect forcings from the three main anthropogenic aerosol species:  $SO_4$ , BC and POM. As evident from Fig. 5a,  $SO_4$  generally has a net cooling effect on the Earth-atmosphere system (global and annual mean of  $\sim -0.15 W m^{-2}$ ). Exceptions are over China, where a major fraction of atmospheric  $SO_4$  is internally mixed with BC and therefore adds to the absorption optical depth, and in the Arctic, where the surface is bright and aerosol particles are generally mixed. In contrast the sulfate indirect forcing is negative everywhere (Fig. 5b), and accounts for about 60% of the total aerosol indirect effect shown in Fig. 4c.

The strong warming effect that BC particles have on the Earth-atmosphere system, amounting to a positive radiative forcing of about  $0.4 W m^{-2}$  on a global and annual average, is shown in Fig. 5c. Maximum values are located over the key industrial regions; Asia, Europe and Eastern USA. However, BC makes practically no contribution to the total aerosol indirect effect. The global and annual average BC indirect forcing amounts to only about  $0.01 W m^{-2}$ . Fig. 5d confirms that the BC indirect forcing is weak, and also exhibits opposite signs in different regions. In a mixed aerosol particle, BC has two opposing effects: it adds mass to the particle but lowers the hygroscopicity. The latter effect seems to dominate in most cases.

Finally, the POM direct forcing is negative practically everywhere (Fig. 5e, global and annual mean of  $\sim -0.25 W m^{-2}$ ), and in magnitude it reaches maxima over the major biomass burning regions in Africa, South-America and Asia. The indirect forcing from POM is also generally negative (Fig. 5f), with the exception of Siberia and Alaska. These regions had major emissions from forest fires around 1850, so the PD emission inventory actually has lower POM emissions here than the PI one. On a global and annual average, POM contributes about 40% of the total aerosol indirect effect.

### 3.4. Changes in aerosol radiative forcings in response to modified entrainment

Also presented in Table 2 are the changes in the total aerosol direct and indirect effects between simulations  $ENT_{HGH}$  and  $ENT_{LOW}$ . Figs. 6 and 7 show the geographical distributions of changes in response to increased entrainment. Evident from Fig. 6a, showing the changes in the direct aerosol effect at the TOA, is that when entrainment is increased, the aerosol direct radiative forcing becomes more positive close to BC source regions (most notably Northeast Asia and African biomass burning regions), and more negative everywhere else. In response to the reduction in internally mixed particles containing BC, more solar radiation is scattered back to space by clouds or bright surfaces. Hence the more negative aerosol direct forcing with increased entrainment, particularly at high northern latitudes where the surface is covered with ice and snow, as well as over the NH storm track. In source regions, however, there are more absorbing aerosols present in the atmospheric column, and consequently a larger fraction of incoming solar radiation is absorbed in the atmosphere and a corresponding smaller fraction of shortwave radiation is scattered back to space.

Changes in the aerosol direct effect at the surface are displayed in Fig. 6b, showing that when entrainment is increased, more solar radiation is absorbed by Earth's surface, leading to a warming everywhere but in confined regions close to sources. The source regions standing out because of their increased aerosol loading and therefore less solar radiation reaching the surface are N.-E. Asia, Eastern US and parts of Europe. Regional changes in the direct aerosol effect in response to increased entrainment exceed  $1 W m^{-2}$ , a

**Fig. 4.** Annual average a) aerosol direct effect, TOA, calculated as the change in net radiative forcing at the TOA (when no indirect aerosol effects are included) between the PD and PI control simulations (PD–PI), b) aerosol direct effect, surface, calculated as in a), but at the surface rather than TOA, and c) aerosol indirect effect calculated by subtracting the shortwave cloud forcing in the PI CTL simulation from the PD CTL simulation.

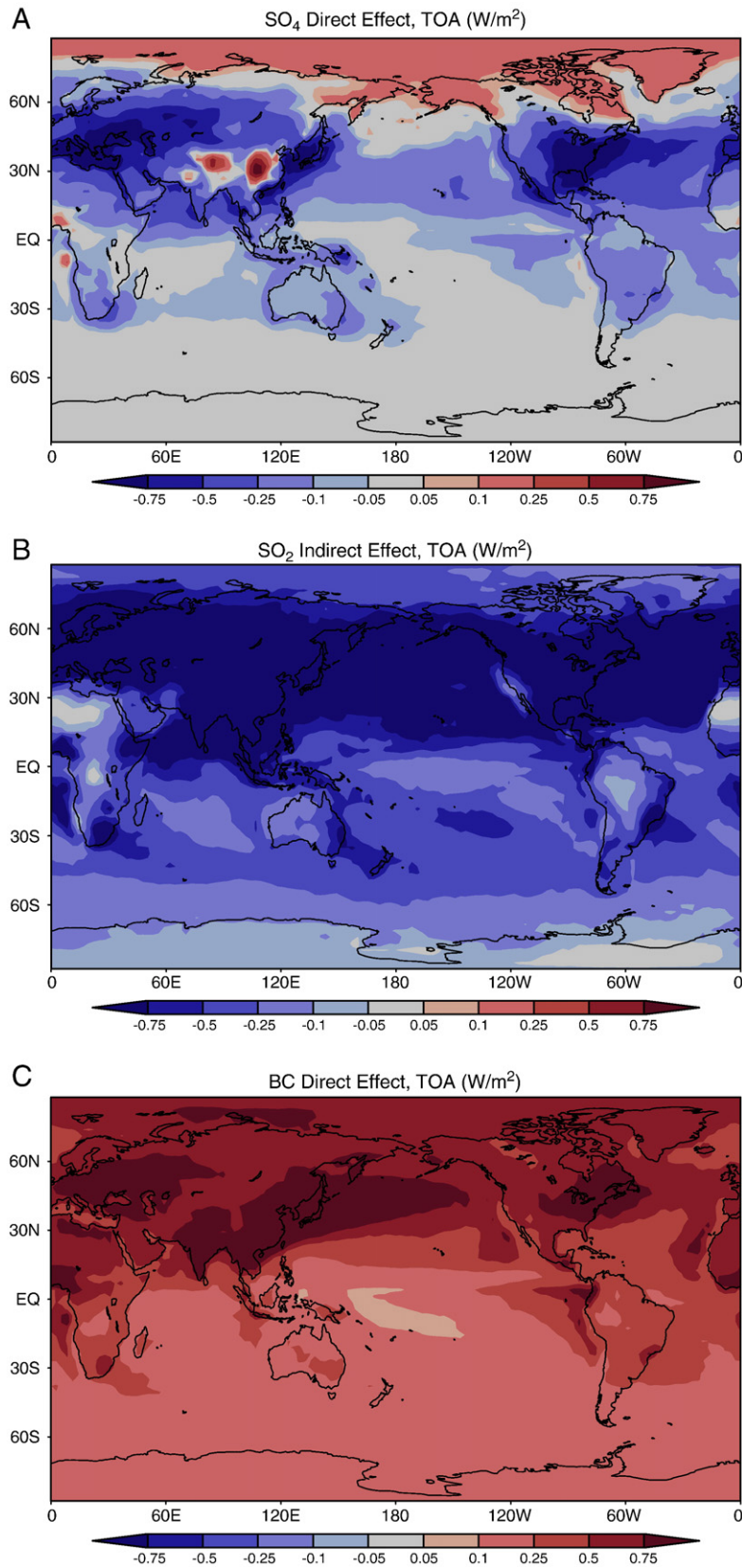


Fig. 5. Annual average direct and indirect effects (in  $\text{W m}^{-2}$ ) for SO<sub>4</sub> (a and b), BC (c and d) and POM (e and f).

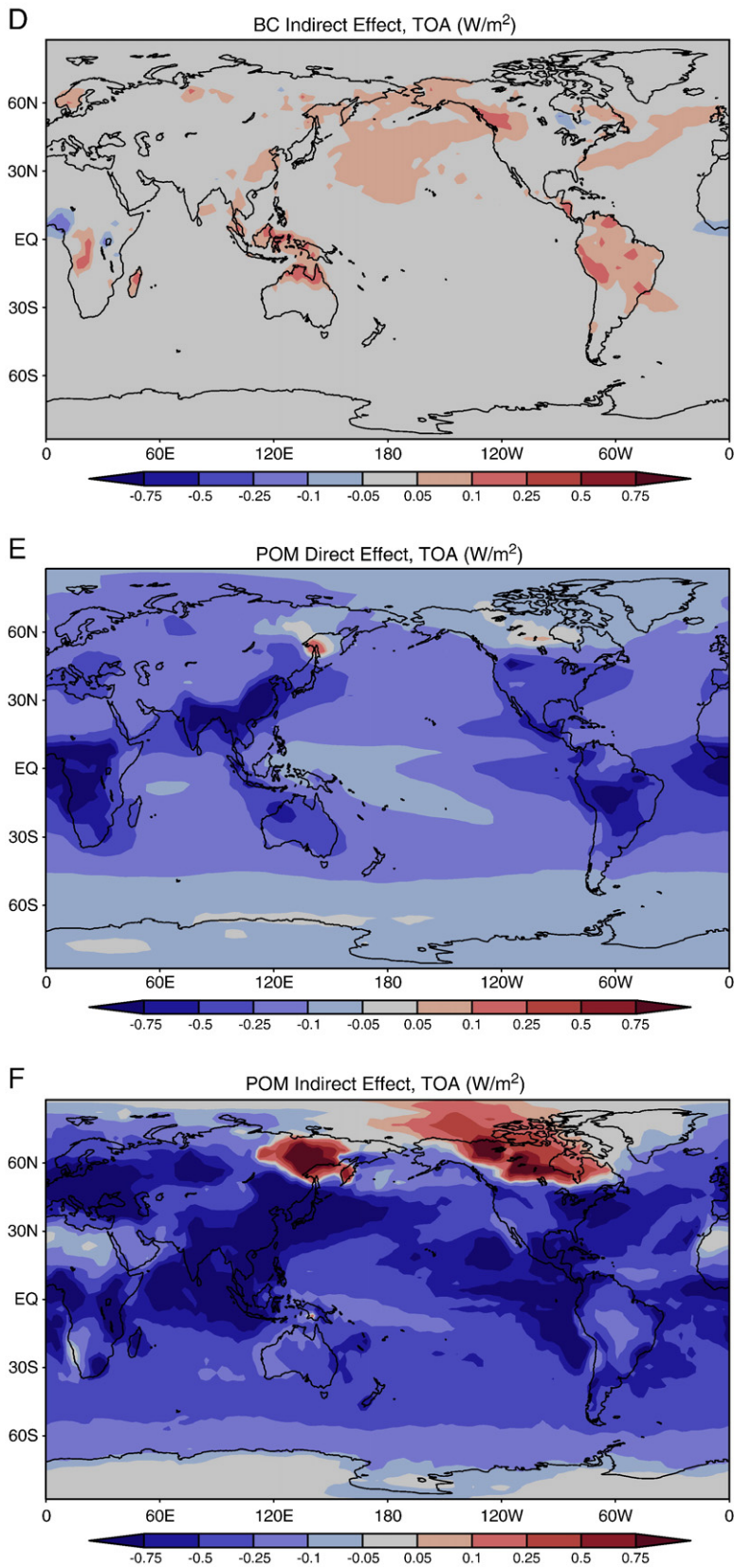
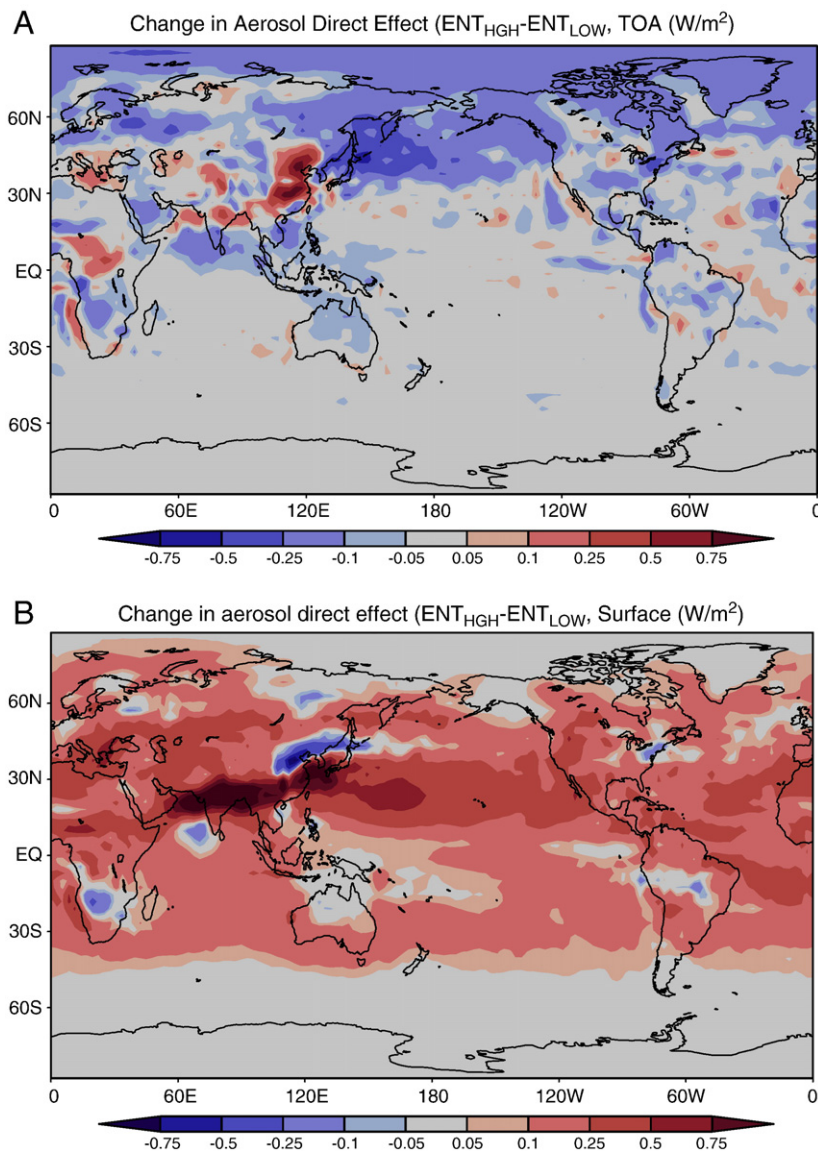


Fig. 5 (continued).



**Fig. 6.** Annual average changes in the aerosol direct effect ( $W m^{-2}$ ) a) at the TOA and b) at the surface, due to increased entrainment in deep convective clouds ( $ENT_{HGH} - ENT_{LOW}$ ).

forcing comparable in magnitude to the positive radiative forcing associated with the increasing  $CO_2$  concentrations in the atmosphere. For prediction of regional climate change, forcing uncertainties that are comparable to the forcings themselves are problematic. The relative changes in direct aerosol forcing at the surface (i.e. Fig. 6b versus Fig. 4b) are also significant; over vast regions of the subtropical ocean, the aerosol direct effect is reduced by more than 50%.

Changes in the aerosol indirect effect, displayed in Fig. 7b, show somewhat similar but slightly more complex patterns. However, in contrast to the direct aerosol effect, changes in column aerosol loading are not necessarily a good predictor for the change in the AIE. Important for a significant change in the AIE is that changes in aerosol concentrations coincide with regions of liquid clouds. In the Tropics, liquid clouds extend well into the free troposphere, and coincide with

regions of strong reduction in aerosol concentrations. As a consequence, cloud albedo is reduced when entrainment is increased, apart from source regions where the increase in boundary layer aerosol concentration compensates for the aerosol reduction aloft. However, modeled convective transport is not confined to the Tropics, and source regions further north also experience higher aerosol concentrations in the lower troposphere in concert with lower concentrations in the mid- and upper troposphere. At high latitudes, however, temperatures are too low to sustain liquid clouds apart from close to the surface. As a result, the slight increase in lower tropospheric aerosols dominates the cloud response at high northern latitudes. Fig. 7a shows changes in the annual mean cloud droplet number concentrations (CDNCs) within the boundary layer (970 hPa). A comparison of Fig. 7a and 7b shows that regions of reduced cloud albedo largely correspond

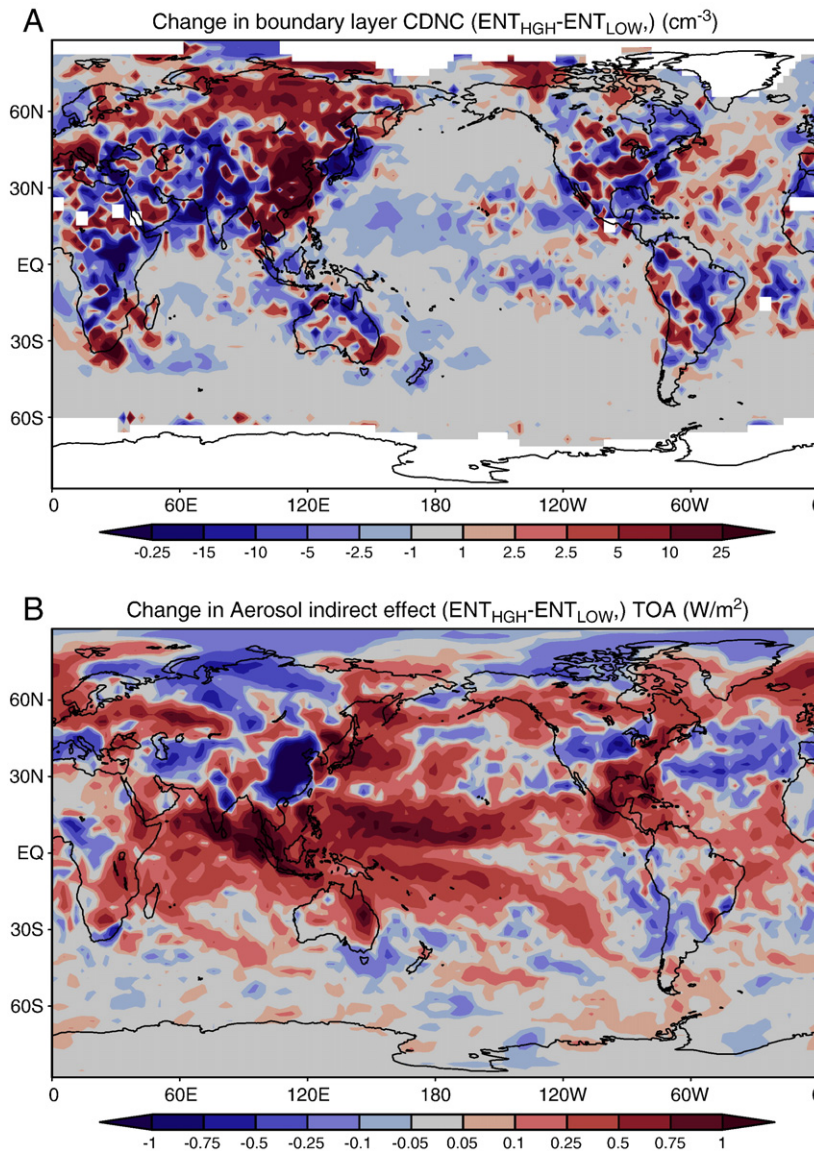


**Fig. 7.** Annual average changes in a) CDNC ( $\text{cm}^{-3}$ ) and b) the aerosol indirect effect ( $\text{W m}^{-2}$ ) due to increased entrainment in deep convective clouds ( $ENT_{HGH} - ENT_{LOW}$ ).

to decreased CDNC in the boundary layer, while the opposite is true for regions with increased cloud albedo. In other words, changes in the concentration of aerosol particles with the ability to act as CCN are largely responsible for the changes in AIE between  $ENT_{HGH}$  and  $ENT_{LOW}$ . Relative to the AIE itself (shown in Fig. 4c), the changes are significant; Tropical and sub-tropical ocean regions and the South-East Asia region experience more than a 50% reduction in the AIE in response to increased entrainment. Eastern USA, which stands out as one of the regions with the strongest reduction in the AIE in Fig. 7b, shows weaker relative changes because this is a region characterized by strong AIE (Fig. 4c). Note that the lower tropospheric cloud cover (including all clouds below the 700 hPa level) increases with increasing entrainment. The global mean difference between  $ENT_{HGH}$  and  $ENT_{LOW}$  is less than 1%, but larger differences are observed regionally. Generally the aerosol indirect effect increases with increasing

cloud cover in the lower troposphere (e.g. (Menon et al., 2002)), which could influence our results.

#### 4. Discussion and conclusion

Global model simulations have been carried out in order to study the sensitivity of global and regional aerosol effects to changes in deep convective entrainment. While globally averaged changes in aerosol loadings and aerosol direct and indirect effects are small, the averaging is masking much larger and opposing regional effects. We find that in response to increased entrainment in deep moist convection, aerosol concentrations are decreased in the upper troposphere, as well as in the lower troposphere far from sources. In source regions, boundary layer and lower tropospheric aerosol concentrations are increased. The changes are due to a smaller upward mass flux of aerosols in the convective plumes, as

well as lower levels of neutral buoyancy and entrainment in the case of more diluted plumes.

Source regions for absorbing aerosols are often located in regions with frequent deep moist convection, and it is therefore not surprising that they experience the largest relative changes in response to changing entrainment. Due to the changes in aerosol vertical and horizontal distribution discussed above when entrainment is increased, the aerosol direct radiative forcing becomes more positive at high latitudes and over source regions, and more negative elsewhere. The direct aerosol radiative forcing at the surface becomes less negative (i.e. the change is positive) everywhere except from confined major source regions, with strongest effects at low latitudes. The aerosol indirect effect shows a more complex pattern of change in response to increased entrainment, but generally is reduced everywhere but in the strongest source regions and at high latitudes where liquid clouds do not coincide with the strongest reduction in aerosol concentrations aloft.

Previous studies suggest that the current parameterization scheme for deep convection in NCAR CAM has weaknesses. Recent studies have addressed this issue and provided suggestions for how the convection scheme could be improved (Lawrence and Rasch, 2005), but these improvements still remain to be implemented and validated. The present study demonstrates that the sensitivity of regional aerosol effects to moderate perturbations to the current convection scheme is significant (on the order of 50%). Only one-way interactions between aerosols and convective clouds were considered, i.e. the effect of entrainment in deep convection on aerosol distributions and associated regional climate effects. However, numerous studies have suggested that aerosols may influence the vigor and lifecycle of deep convection (e.g. Rosenfeld and Woodley, 2000; Planche et al., 2010), which in turn may have implications for large-scale circulation (e.g. Emanuel et al., 1994). Furthermore, biomass burning can influence moist convection not only via aerosol emissions, but also by adding a significant heat source at the surface. The particularly intense deep convective clouds sometimes observed in association with biomass burning are also known as pyrocumulii (Andreae et al., 2004), and are not accounted for in this study. Properly accounting for how the heat from biomass burning influences deep convection goes beyond the scope of this study, but certainly represents one interesting extension to it. The issues above, along with the identification of environmental conditions in which deep moist convection is particularly poorly represented in NCAR CAM and potential remedies, will be the subject of future studies. Thanks to recent and upcoming targeted field campaigns, the global modeling community will soon have new observational guidance regarding entrainment rates in deep convection. For example, the recently completed MC3E campaign (<http://campaign.arm.gov/mc3e/>), a collaborative effort between the U.S. Department of Energy and the National Aeronautics and Space Administration (NASA), promised the most complete characterization data set for convective cloud systems that has ever been obtained.

## Acknowledgments

The work presented in this paper was supported in part by the facilities and staff of the Yale University Faculty of Arts and Sciences High Performance Computing Center. The author

is grateful to Trond Iversen, Alf Kirkevåg, Jon Egill Kristjansson, Øyvind Seland and Corinna Hoose for their roles in the development of the aerosol and cloud microphysics modules used in this study. Furthermore, the author is thankful to one anonymous reviewer, whose comments helped improving this manuscript significantly.

## References

- Abdul-Razzak, H., Ghan, S.J., 2000. A parameterization of aerosol activation. part 2: Multiple aerosol types. *J. Geophys. Res.* 105, 6837–6844.
- Andreae, M.O., Rosenfeld, D., Artaxo, P., Costa, A.A., Frank, G.P., Longo, K.M., Silva-Dias, M.A.F., 2004. Smoking rain clouds over the Amazon. *Science* 303, 1337–1342.
- Barth, M., Church, A., 1999. Regional and global distributions and lifetimes of sulfate aerosols from Mexico City and southeast China. *J. Geophys. Res.* 104, 30,231–30,239.
- Benner, T., Curry, J., 1998. Characteristics of small tropical cumulus clouds and their impact on the environment. *J. Geophys. Res.* 103, 28,753–28,767.
- Collins, W., Rasch, P., Boville, B., Hack, J., McCaa, J., Williamson, D., Briegleb, B., Bitz, C., Lin, S., Zhang, M., 2006. The formulation and atmospheric simulation of the Community Atmosphere Model: CAM3. *J. Clim.* 19, 2144–2161.
- Del Genio, A., Wu, J., 2010. The role of entrainment in the diurnal cycle of continental convection. *J. Clim.* 23, 2722–2738.
- Dentener, F., Kinne, S., Bond, T., Boucher, O., Cofala, J., Generoso, S., Ginoux, P., Gong, S., Hoelzemann, J.J., Ito, A., Marelli, L., Penner, J.E., Putaud, J.P., Textor, C., Schulz, M., van der Werf, G., Wilson, J., 2006. Emission of primary aerosols and precursor gases in the years 2000 and 1750 prescribed data-sets for aerocom. *Atm. Chem. Phys.* 6, 4321–4344.
- Emanuel, K.A., Neelin, J.D., Bretherton, C.S., 1994. On large-scale circulations in convecting atmospheres. *Q. J. R. Meteorol. Soc.* 120, 1111–1143.
- Forster, P., Ramaswamy, V., Artaxo, P., Bernsten, T., Betts, R., Fahey, D., Hay, J., Lean, J., Lowe, D., Myhre, G., Nganga, J., Prinn, R., Raga, G., Schulz, M., Van Dorland, R., 2007. Changes in Atmospheric Constituents and in Radiative Forcing. *Climate Change 2007: The Physical Science Basis. Contribution of Working Group I to the Fourth Assessment Report of the Intergovernmental Panel on Climate Change.* Cambridge University Press, Cambridge, United Kingdom and New York, NY, USA.
- Grabowski, W.W., 2001. Coupling cloud processes with the large-scale dynamics using the Cloud-Resolving Convection Parameterization (CRCP). *J. Atmos. Sci.* 58, 978–997.
- Grabowski, W.W., Bechtold, P., Cheng, A., Forbes, R., Halliwell, K., Khairoutdinov, M., Lang, S., Nasuno, T., Petch, J., Tao, W.K., Wong, R., Wu, X., Xu, K.M., 2006. Daytime convective development over land: a model intercomparison based on LBA observations. *Q. J. R. Meteorol. Soc.* 132, 317–344.
- Grabowski, W.W., Moncrieff, M.W., 2004. Moisture-convective feedback in the tropics. *Q. J. R. Meteorol. Soc.* 130, 3081–3104.
- Gustafson, W., Berg, L., Easter, R., Ghan, S., 2008. The explicit-cloud parameterized-pollutant hybrid approach for aerosol–cloud interactions in multiscale modeling framework models: tracer transport results. *Environ. Res. Lett.* 3, 025005.
- Kirkevåg, A., Iversen, T., 2002. Global direct radiative forcing by process-parameterized aerosol optical properties. *J. Geophys. Res.* 105. <http://dx.doi.org/10.1029/2001JD000886>.
- Lawrence, M.G., Rasch, P.J., 2005. Tracer transport in deep convective updrafts: plume ensemble versus bulk formulations. *J. Atmos. Sci.* 62, 2880–2894.
- Lohmann, U., Rotstain, L., Storelvmo, T., Jones, A., Menon, S., Quaas, J., Ekman, A.M.L., Koch, D., Ruedy, R., 2010. Total aerosol effect – radiative forcing or radiative flux perturbation? *Atm. Chem. Phys.* 10, 3235–3246.
- Mahowald, N., Rasch, P.J., Eaton, B.E., Whittlestone, S., Prinn, R.G., 1997. Transport of radon to the remote troposphere using the model of atmospheric transport and chemistry and assimilated winds from ECMWF and the national center for environmental prediction/NCAR. *J. Geophys. Res.* 102, 28,139–28,151.
- Maloney, E.D., Sobel, A.H., Hannah, W.M., 2010. Intraseasonal variability in an aquaplanet general circulation model. *J. Adv. Model. Earth Syst.* 2 (Art. #5), 24. <http://dx.doi.org/10.3894/JAMES.2010.2.5>.
- Menon, S., Del Genio, A.D., Koch, D., Tselioudis, G., 2002. GCM simulations of the aerosol indirect effect: sensitivity to cloud parameterization and aerosol burden. *J. Atmos. Sci.* 59, 692–713.
- Planche, C., Wobrock, W., Flossmann, A.I., Tridon, F., Van Baelen, J., Pointin, Y., Hagen, M., 2010. The influence of aerosol particle number and hygroscopicity on the evolution of convective cloud systems and their precipitation: a numerical study based on the COPS observations on 12 August 2007. *Atm. Res.* 98, 40–56.
- Pruppacher, H.R., Klett, J.D., 1997. *Microphysics of clouds and precipitation.* Kluwer Academic.

- Raymond, D.J., Blyth, A.M., 1986. A stochastic mixing model for non-precipitating cumulus clouds. *J. Atmos. Sci.* 43, 2708–2718.
- Raymond, D.J., Blyth, A.M., 1992. Extension of the stochastic mixing model to cumulonimbus clouds. *J. Atmos. Sci.* 49, 1968–1983.
- Riemer, N., West, M., Zaveri, R., Easter, R., 2010. Estimating black carbon aging time scales with a particle-resolved aerosol model. *J. Aero. Sci.* 41, 143–158.
- Rosenfeld, D., Woodley, W.L., 2000. Deep convective clouds with sustained supercooled liquid water down to  $-37.5$  degrees C. *Nature* 405, 440–442.
- Schulz, M., Textor, C., Kinne, S., Balkanski, Y., Bauer, S., Bernsten, T., Berglen, T., Boucher, O., Dentener, F., Guibert, S., Isaksen, I., Iversen, T., Koch, D., Kirkevåg, A., Liu, X., Montanaro, V., Myhre, G., Penner, J., Pitari, G., Reddy, S., Seland, Ø., Stier, P., Takemura, T., 2006. Radiative forcing by aerosols as derived from the AeroCom present-day and pre-industrial simulations. *Atmos. Chem. Phys.* 6, 5225–5246.
- Seland, O., Iversen, T., Kirkevåg, A., Storelvmo, T., 2008. Aerosol-climate interactions in the CAM-OSLO atmospheric GCM and investigation of associated basic shortcomings. *Tellus* 60A, 459–491.
- Siebesma, A.P., Jonker, H.J.J., 2000. Anomalous scaling of cumulus cloud boundaries. *Phys. Rev. Lett.* 85, 214–217.
- Small, J.D., Chuang, P.Y., Feingold, G., Jiang, H., 2009. Can aerosol decrease cloud lifetime. *Geophys. Res. Lett.* 36. <http://dx.doi.org/10.1029/2009GL038888>.
- Stevens, B., Feingold, G., 2009. Untangling aerosol effects on clouds and precipitation in a buffered system. *Nature* 461, 607–613.
- Storelvmo, T., Kristjánsson, J.E., Ghan, S.J., Kirkevåg, A., Seland, Ø., Iversen, T., 2006. Predicting cloud droplet number concentration in community atmosphere model (cam)-oslo. *J. Geophys. Res.* 111.
- Textor, C., Schulz, M., Guibert, S., Kinne, S., Balkanski, Y., Bauer, S., Bernsten, T., Berglen, T., Boucher, O., Chin, M., Dentener, F., Diehl, T., Easter, R., Feichter, H., Fillmore, D., Ghan, S., Ginoux, P., Gong, S., Grini, A., Hendricks, J., Horowitz, L., Huang, P., Isaksen, I., Iversen, T., Kloster, S., Koch, D., Kirkevåg, A., Kristjánsson, J.E., Krol, M., Lauer, A., Lamarque, J.F., Liu, X., Montanaro, V., Myhre, G., Penner, J., Pitari, G., Reddy, S., Seland, Ø., Stier, P., Takemura, T., Tie, X., 2006. The effect of harmonized emissions on aerosol properties in global models Ð an AeroCom experiment. *Atmos. Chem. Phys.* 6, 1777–1813.
- Zhang, G., McFarlane, N., 1995. Sensitivity of climate simulations to the parameterization of cumulus convection in the Canadian Climate Centre general circulation model. *Atmos. Ocean* 33, 407–445.